FINITE ELEMENT MODELING A FULL SCALE ADJACENT PRESTRESSED CONCRETE BOX BEAM BRIDGE SPAN

Jonathan Huffman, MS, Grad. Research Assistant, Civil Engineering, Ohio University, Athens, OH
Eric Steinberg, PhD, PE, Associate Professor, Civil Engineering, Ohio University, Athens, OH
Shad Sargand, PhD, Professor, Civil Engineering, Ohio University, Athens, OH

ABSTRACT

A finite element model (FEM) was constructed for a 43 year old adjacent prestressed concrete box beam bridge span. The model was used to validate results acquired during the full-scale destructive testing of a damaged span. Damage to the actual span was created to simulate three extremely deteriorated interior beams within the span.

The model of the bridge span consisted of adjacent reinforced concrete box beams, shear keys, and appropriate boundary conditions to model the effects of the transverse tie rods and supports. The behavior of the concrete was modeled using non-linear material properties. The damage of the span was modeled by altering the input parameters for the concrete of the damaged sections.

Once the model was constructed, loadings similar to those applied during the destructive test were placed on the model. The strains and deflections found using the FEM yielded similar results relative to the actual testing conducted on the span. The damage was removed from the model and results from static truck testing conducted prior to the bridge being damaged were also simulated. This modeling assisted in determining load distribution factors for the span, and will assist in the evaluation of other bridges with varying degrees of damage.

Keywords: Bridge Modeling, Finite Element Modeling, Damaged Bridge Span, Adjacent Box Beams, Live Load Distribution

INTRODUCTION

During analysis of the results obtained from a full-scale destructive test of a 43 year old damaged prestressed adjacent box beam bridge span, unusual trends between the strain and deflections results on the damaged beams were observed[1,2]. To help explain the unusual behavior and validate the results of the testing a non-linear finite element model (FEM) was created using Abaqus/CAE 6.10 to simulate the response of the damaged bridge span during testing.

The FEM created for the damaged bridge span was a full-scale three-dimensional model with no geometric or symmetric simplifications to the bridge span cross-section. The model consisted of nine adjacent box beams with all longitudinal reinforcement and eight shear keys. The abutment and pier supports were modeled by using a combination of boundary conditions and axial springs. Similarly, the transverse tie rods connecting the beams together were also modeled through the use of axial springs. The concrete components of the bridge span were modeled using non-linear material properties to account for the post-cracking behavior of the concrete.

The damage induced on the actual bridge span consisted of two cuts into the bottom flanges of three interior beams at 23.7 ft and 27 ft from the end of the beams. The cuts severed the entire bottom row of prestressed reinforcement of the beams. The damage was created to simulate severe deterioration of the interior beams. The damaged sections of the three interior beams were modeled in the FEM by substituting the material properties of the damaged cross-sections with an elastic material, of relatively low stiffness. The bottom row of longitudinal reinforcement was also removed from the damaged sections of the concrete.

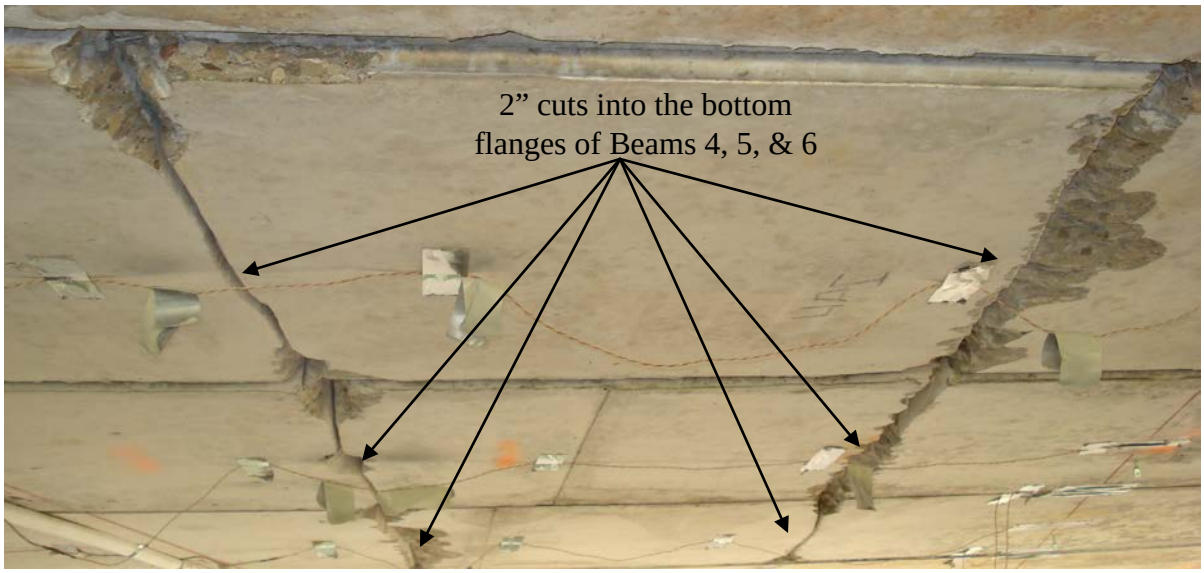

Figure 1 – Damaged created on 3 interior beams

The loading procedure completed during the destructive testing of the actual bridge span was simulated in the FEM by placing a group of point loads at the locations used during the field testing. These locations consisted of three loading regions each approximately 4 ft x

1 ft, which represented the field loading on the bridge span by hydraulic cylinders. The cylinders were labeled by which beam was directly beneath the cylinder spreader beams.

Once the FEM was assembled, it was then calibrated to match the behavior of the results from the destructive testing conducted on the actual bridge span while the three damaged interior beams were subjected to loading. To justify these results, the model was then loaded at the other two loading locations at the same magnitudes as recorded during field testing. Then minor modifications to the FEM were made to further calibrate the model to better simulate the behavior of the span when loaded at any location. Once fully calibrated, all three loading conditions were repeated and the results recorded. The results were then compared to results from the destructive testing of the damaged bridge span.

To further validate the effectiveness of the FEM at simulating the span behavior, the simulated damaged sections were removed from the modeled span with no additional alterations to the model. The model was then subjected to four separate truck loadings equivalent to truck testing preformed on the actual bridge span prior to the damage being induced on the span. The FEM results were then compared to the results from the truck testing conducted on the bridge span[3].

BACKGROUND

The concepts behind non-linear finite element analysis and modeling have been available for several decades; however the use of finite element analysis has not been a plausible solution for large structural systems because of the associated cost of the computational resources required to conduct such a large analysis. With the advancement in computational technologies, using finite element as an analytical tool to evaluate and model large structural systems is now readily available.

The use of non-linear FEM is frequently used in modeling the behavior of reinforced concrete. The advantages of non-linear FEM are that the linear and non-linear behavior concrete can be accurately modeled. Concrete behaves linearly at low stress levels (<30-40% of ultimate). The non-linear behavior at higher stress levels is due to micro cracking at the interface of the cement and aggregate[4]. With non-linear FEM, the effects of micro and macro cracking in the concrete are included in the analysis.

In non-linear FEM there are many variables that influence the accuracy of a reinforced concrete model. In order to correctly evaluate the failure mechanism(s) of a particular reinforced concrete structure, element type, mesh size, load step, convergence criteria, presence or absence of bond-slip, and material properties should be appropriately chosen[5]. When modeling concrete, several characteristics of the concrete should be considered. This includes cracking criteria, tension stiffening, tension softening, compression hardening, compressive ductility, compression softening, multi-directional cracking, relation of shear stiffness to cracking, and multi-axial stress conditions[5]. Modeling the concrete using a smeared cracking method is the predominate approach used in three-dimensional modeling of concrete[6].

In a smeared cracking model the effects of the non-linear compressive and tensile behaviors of the concrete are taken into account. Abaqus/CAE uses a smeared cracking model that simplifies the compressive and tensile behaviors of the concrete into piece-wise

linear stress-strain curves. These curves account for the compression hardening and softening as well as loss of tensile strength upon cracking and tension stiffening. The actual cracking in the concrete is not tracked in a smeared cracking model. Once the criterion for cracking has been met for a particular element, the appropriate material properties are applied to the individual element. The effect of the crack is considered "smeared" throughout the element. The altered material property of the element will also change the stresses in the surrounding elements which may cause additional elements to crack, further smearing the effect of the crack.

MODEL CONSTRUCTION

A full-scale finite element model was constructed to analyze the results of the severely damaged span of the field tested bridge. A non-linear three-dimensional model was constructed in Abaqus/CAE 6.10 composed of nine adjacent box beams with longitudinal reinforcement and eight shear keys. The prestressed concrete box beams were modeled using a smeared cracking method with the reinforcement modeled as embedded solid elements.

COMPONENTS

The cross-sections of the precast concrete box beams, beam solid sections, prestressed reinforcement, conventional reinforcement, and shear keys of the bridge span were drawn in the Abaqus/CAE to the specifications provided in the bridge design drawings. The beam solid sections of the precast beams were drawn separately to make meshing the two parts possible in a practical manner. Once the cross-sections were drawn, the box beams, prestressed reinforcement, conventional reinforcement, and shear keys were extruded 574 in. (47'10") in the longitudinal direction to match the length of the bridge span. The beam solid sections were extruded to yield two solid sections at the location of the transverse tie rods for each box beam. The actual length of the solid sections in each beam was not specified in the bridge design drawings therefore a value of 18 in. was assumed.

Each of the components were seeded six inches along the length and then meshed independently. This created 7,081 elements for each beam, 2,496 elements per shear key, and 2976 elements for the reinforcement in each beam. An illustration of the mesh resolution of a single box beam can be seen in Figure 2.

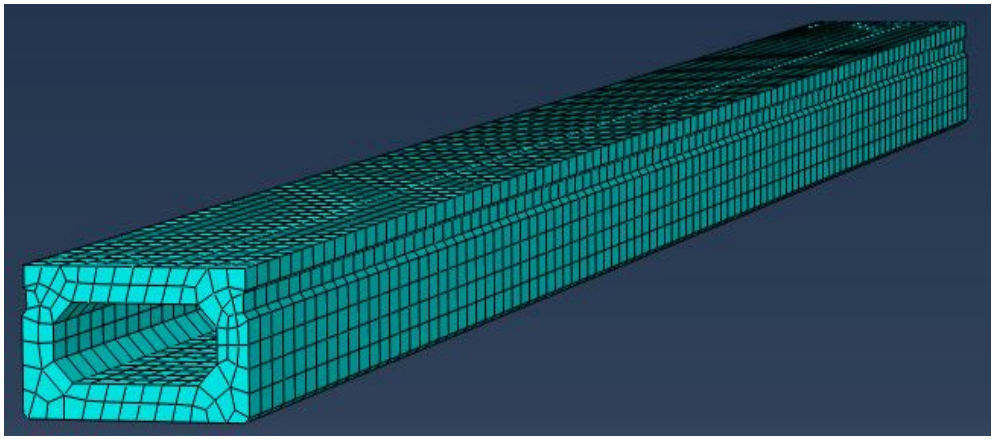

Figure 2 – Mesh resolution of a beam

MATERIALS

The elastic concrete material properties were modeled by defining the Young's modulus and Poisson's ratio for the concrete. Several cores taken from the east span of the bridge were tested. The tests yielded a compressive concrete strength of 10 ksi, a Poisson's ratio of 0.2, and a unit weight of 147 pcf. These values were used in modeling the material properties of the beams and shear keys[3]. The solid sections of each beam were assigned the same material properties as the corresponding beam. It should be noted that a concrete compressive strength of 10 ksi was not used for all of the concrete parts. A complete list of the material properties for each part is provided in Table 1. The compressive strength of several concrete parts was changed to improve the model behavior to compare with test results.

Table 1 - FEM Material Properties

	Material Property		
Part	f'_c (ksi)	E (ksi)	ν
Beams 1,2,3,7,9	10	5882	0.2
Beams 4, 5, 6, 8	14	6959	0.2
Shear Keys	10	5882	0.2

The plastic concrete material properties were defined using a concrete smeared cracking model. To define the concrete smeared cracking material properties, post-yield compressive and tensile stress-strain relations were defined, as were failure ratios for the concrete.

For the compressive stress-strain relationship, a list of compressive stresses and the associated plastic strains were input. To define the tensile stress-strain relation, a list of the tensile stress after cracking to tensile stress at cracking ratios ($\frac{\sigma_{tac}}{\sigma_{tc}}$), and the corresponding strain after cracking to strain at cracking ratios ($\frac{\varepsilon_{tac}}{\varepsilon_{tc}}$) were input. Equations were developed that allowed all parameters of the post-yield compressive and tensile stress-strain relationships to be defined by setting a single concrete compressive strength. These equations were developed by combining equations and relationships discussed in *Reinforced Concrete, Mechanics and Design*[4] as well as relationships provided in the Abaqus Analysis User's Manual[7]. The equations and relationships are listed in Eqs. 1-7:

Young's Modulus: $$E_c = w^{1.5} * 33\sqrt{f'_c} \quad \text{(Eq. 1)}$$

Where: $w = unit\ weight\ of\ concrete$

$f'_c = compressive\ strength\ of\ concrete$

Factored Compressive Strength: $$f''_c = 0.9 f'_c \quad \text{(Eq. 2)}$$

Compressive Strain at Yield: $\varepsilon_{cy} = 1.8\frac{f''_c}{E_c}$ (Eq. 3)

Tensile Strength: $f'_t = R_2 f'_c$ (Eq. 4)

Where: $R_2 = Failure\ Ratio\ 2$

Tensile Strain at Yield: $\varepsilon_{ty} = 1.8\frac{f'_t}{E_c}$ (Eq. 5)

Compressive Stress at Failure: $f'_{cult} = 0.85 f'_c$ (Eq. 6)

Compressive Strain at Failure: $\varepsilon_{cult} = 0.0038\ \frac{in}{in}$

Tensile Strain at Failure: $\varepsilon_{tult} = 10 * \varepsilon_{ty}$ (Eq. 7)

The compressive and tensile stress-strain diagrams in Figure 4 represent the limits of the concrete smeared cracking material properties. The stress-strain curves shown are based on a compressive strength of 10 ksi. The relationships in the stress-strain diagrams were derived from relationships discussed in the Abaqus Analysis User's Manual[7].

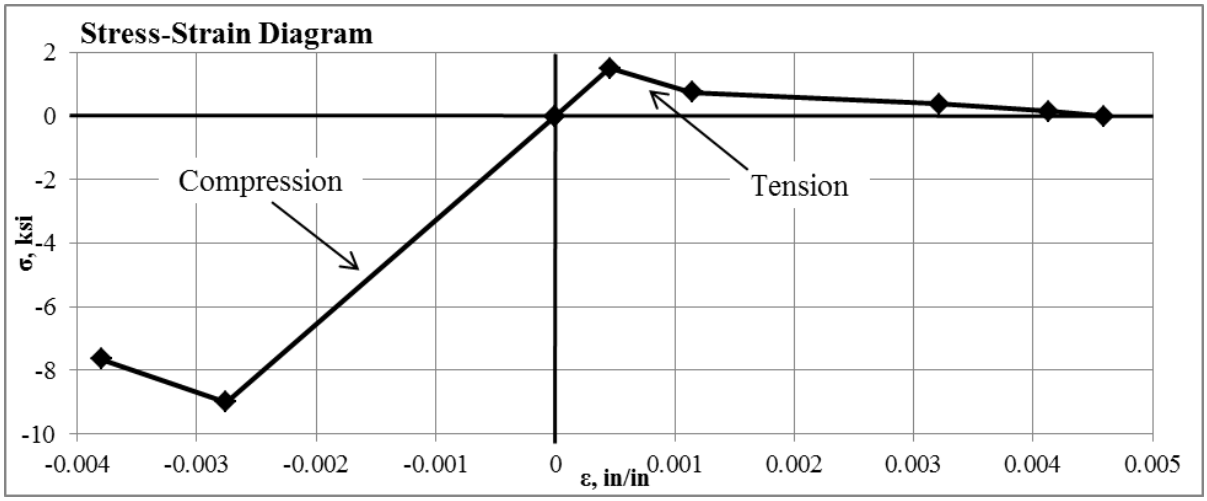

Figure 4 – Compressive and Tensile stress-strain curve

Four failure ratios were defined for the smeared cracking concrete material method. The definitions and default values provided in the Abaqus/CAE User's Manual[8] are listed in Table 2. For this model, the default values were used for ratios 1, 3, and 4 because further testing of the concrete being modeled was not available. Ratio 2 was changed from the default value of 0.09 to 0.15 to allow for quicker convergence in the full analysis of the bridge model.

Table 2 – Failure Ratios as defined in Abaqus/CAE User's Manual[8]

Ratio	Definition	Default Value
1	Ratio of the ultimate biaxial compressive stress to the uniaxial compressive ultimate stress.	1.16
2	Absolute value of the ratio of uniaxial tensile stress at failure to the uniaxial compressive stress at failure.	0.09
3	Ratio of the magnitude of a principal component of plastic strain at ultimate stress in biaxial compression to the plastic strain at ultimate stress in uniaxial compression.	1.28
4	Ratio of the tensile principal stress value at cracking in plane stress, when the other nonzero principal stress component is at the ultimate compressive stress value, to the tensile cracking stress under uniaxial tension.	0.33

The prestressed and conventional reinforcement material properties were defined using the same material properties. The reinforcement was modeled as an elastic material with a Young's modulus of 29,000 ksi, and a Poisson's ratio of 0.3. The prestress of the strands was not included in this analysis because the results from the destructive testing were relative to the behavior after the prestressing.

DAMAGE

The damage was modeled by taking a three inch long cross-section from the beams at the location of the induced damage and replacing the concrete material properties with an elastic material that had a relatively low Young's modulus and a relatively high Poisson's ratio. The Young's modulus and Poisson's ratio differed for each damaged section. Table 3 presents the material properties used in the damaged sections. Sections labeled (A) are the material properties for the cross-section modeling the cut made 23.7 ft from the bridge abutment and sections labeled (B) are the properties for the cross-section modeling the cut made 27 ft from the bridge abutment. These values differ significantly in the damaged cross-sections to model the behavior observed in the results from the bridge span testing. Also, the 14 prestressed strands of the bottom row in the damaged beams were cut so that these strands were not present in the 3 in. damaged cross-sections. The material in the damaged sections models the formation of a plastic hinge when the load is applied to the bridge model. Manipulating these damaged sections allowed the strain discontinuity between the damaged and undamaged beams to be accurately modeled.

Table 3 - Material properties of the damaged sections

Part	Young's Modulus (ksi)	Poisson's Ratio
Beam 4 Damage (A)	600	0.30
Beam 4 Damage (B)	300	0.30
Beam 5 Damage (A)	40	0.30
Beam 5 Damage (B)	*6959	*0.20
Beam 6 Damage (A)	10	0.30
Beam 6 Damage (B)	1400	0.30

* - Material properties were not changed and were the same as the beam

INTERACTIONS

The interaction between the concrete beam and the reinforcement was modeled as an embedment constraint. Embedding the elements of the reinforcement in the concrete elements is an effective computational method to accurately model the effect of the reinforcement on the surrounding concrete elements[5]. The embedment constraint embeds a group of user defined non-host elements into a group of user defined host elements. The sets of steel reinforcement were defined as non-host elements and the individual beams were defined as the host elements. When a group of non-host elements is embedded in a group of host elements, the translational degrees of freedom of the non-host elements are taken away where the nodes of the non-host elements coincide with the nodes of the host elements. The translations at each degree of freedom of nodes of the host elements are then placed on the nodes of non-host elements. This assumes there is non-slip bonding between the concrete and reinforcement. Slip and non-slip bonding in embedded steel reinforcement was investigated by Barzegar and Maddipudi; it was concluded that the global behavior did not significantly change when accounting for bond-slip[5]. This particular embedment type is solid element embedded into solid element. This will result in a more accurate modeling of the concrete-reinforcement interaction as opposed to modeling the reinforcement as shell or membrane elements. However, using shell or membrane elements is more computationally economical.

For the interaction between the beam solid sections and the hollow box beams, the outer perimeter surfaces of the beam solid sections were tied to the inner perimeter of the box beams using a surface to surface tie constraint. This constraint bonds the two surfaces together absolutely. This models a perfect bond between the two surfaces, and since the actual solid sections of the beams were precast monolithically with the beams this is an appropriate method to bond the two surfaces.

The interaction between the concrete beams and the shear keys was also modeled using a surface to surface contact. The surfaces of the shear keys and beams that come into contact were defined as contact pairs. Both the tangential and normal behaviors of the surface contact were defined. The friction formulation was defined in the tangential behavior and a coefficient of friction (μ). The normal behavior was selected to be linear and was given a contact stiffness which controls the transfer of normal stresses between the two surfaces of the contact. The contact stiffness also restrains the nodes of the two contacting surfaces from penetration into one another. The values given for the coefficient of friction and the contact stiffness varied to model the distribution of strain and deflection transversely across the actual bridge span. The values used for the coefficient of friction and contact stiffness for each interaction are listed in Table 4.

Table 4 -Varied interaction properties, μ and K_c

Interaction	Coefficient of Friction, μ	Contact Stiffness, K_c
Shear Key 1-2	0.60	35
Shear Key 2-3	1.00	150
Shear Key 3-4	0.85	100
Shear Key 4-5	0.80	100
Shear Key 5-6	0.80	100
Shear Key 6-7	1.00	200
Shear Key 7-8	0.60	10
Shear Key 8-9	0.60	10

In Figure 4, the assembled interaction between the beams and reinforcement and the beams and shear keys can be observed.

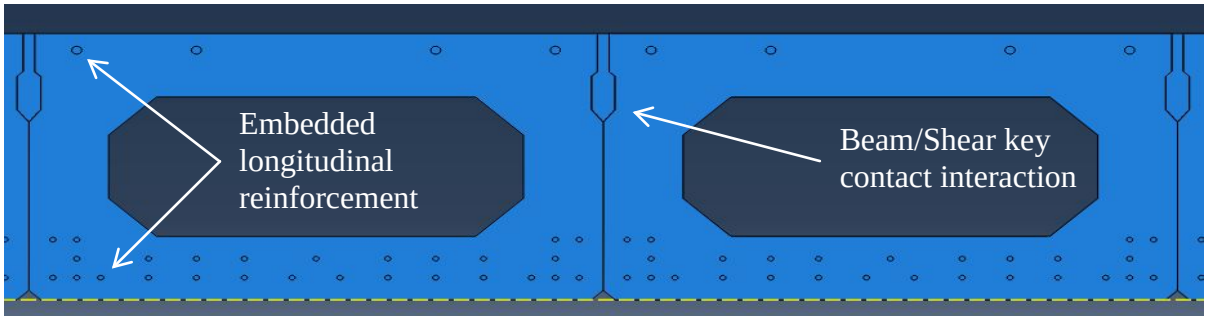

Figure 4 - Assembled cross-section

LOADS

In the damaged bridge span model, surface nodes lying on the top surface of the beams within the location of the cylinder loadings were defined in sets for each of the three cylinder locations. Defining node sets at the locations of the actual cylinder locations allowed for accurate modeling of the behavior of the load applied in the destructive testing of the bridge span. Once the sets were defined for each loading location, the desired magnitude of load to be applied to the model was divided by the number of nodes for that cylinder node set and concentrated point loads were applied at each node of the node set in the downward vertical direction. Figure 5 provides a plan view of the FEM showing the load applied at the node sets for all of the cylinders.

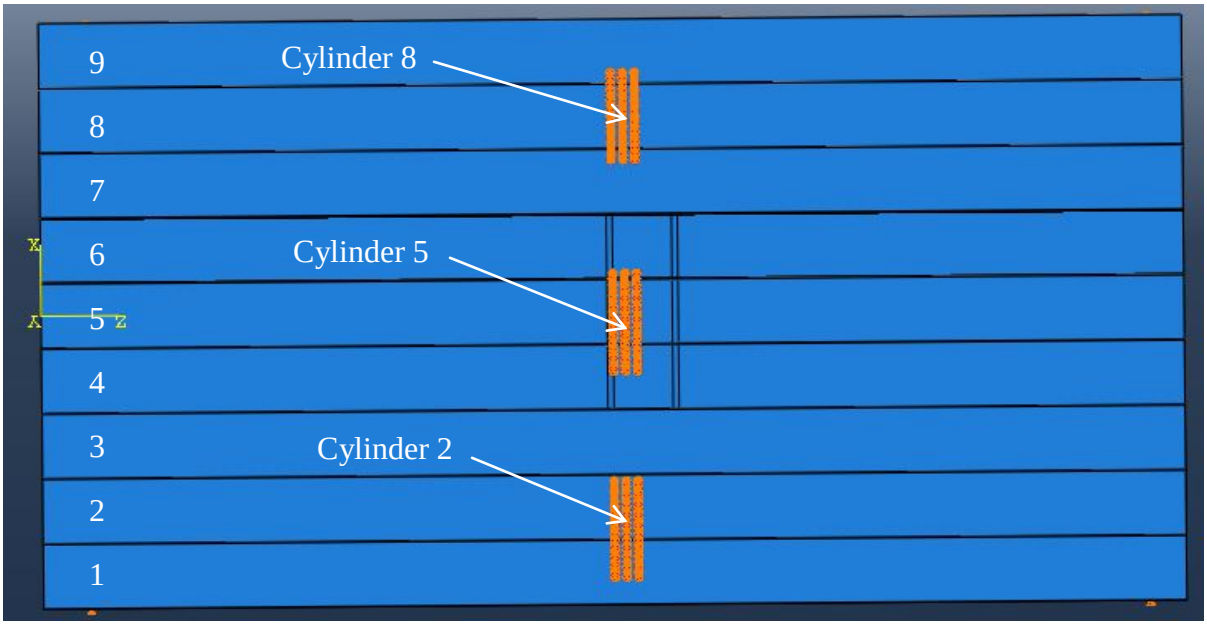

Figure 5 – Cylinder load locations on the damaged bridge span model

Similar to the cylinder loadings on the damaged bridge span model, the truck loads were applied to the undamaged bridge span model by applying concentrated loads to the nodes that were located on the top surface of the beams where the tires contacted the bridge span. The magnitude of load applied at each tire load location corresponded with the load from each tire that was measured during the truck load testing of the bridge span. Figures 6 and 7 shows the locations of the tire loads for each of the four truck loadings modeled with the undamaged bridge span model.

Figure 6 – Truck loading locations 1 and 2 on the undamaged bridge span model

Figure 7 – Truck loading locations 3 and 4 on the undamaged bridge span model

BOUNDARY CONDITIONS

To model the abutment and pier of the damaged bridge span, a combination of support conditions and axial springs were used. For the abutment, a node set was defined 18 in. from the end of the beam on the bottom surface of the beam. This node set contained 13 evenly spaced nodes per beam, and a complete transverse translational restraint was defined for these nodes. The purpose of this restraint was to aid in mathematical convergence of the model and had minimal influence on the results of the model. The effects of the abutment on the translations of the span longitudinally and vertically were accounted for using axial springs. Strict support conditions, such as complete translational restraints, were not used because this also caused mathematical convergence problems. These axial springs were placed 18 in. from the end of the beam. The stiffness of the axial springs was assigned individually for each beam to allow for differences in the influence of the dowel bars in the abutment on each beam.

The effects of the pier on the bridge span were modeled similarly to the abutment. However, the location of the node sets for the complete transverse translational restraint and axial springs were located 12 in. rather than 18 in. from the end of the beam.

TRANSVERSE TIE RODS

The transverse tie rods were modeled in the damaged bridge span with axial springs. The adjacent nodes of adjacent beams at the location of the transverse tie rods were tied together using springs. This axial spring caused the force due to the translations in the transverse, vertical, and longitudinal directions of one node to be transferred to the adjacent node on the adjacent beam. The reaction of the axial springs when the span was loaded resulted in a concentrated force on the nodes where the axial springs were applied. This reaction allowed for the development of a normal force required for the tangential behavior in the interaction between the shear keys and beams.

RESULTS

Once an accurate FEM was produced, the strain and deflection results output by the model were compared to the results of three selected loading cases obtained during the destructive testing of the bridge span. The loading cases selected were taken from the single cylinder loading of the bridge span. The first loading case was when Cylinder 2 was applying 62.3 kips, the second was when Cylinder 5 was applying 72.7 kips, and the final loading case was when Cylinder 8 was applying 51.9 kips. The results from the FEM and experimental results are for the strain and deflections recorded at two instrument lines that ran transversely across the bridge span. The first instrument line was located 22 ft from the end of the beams (Line MS & MD). The second instrument line was located 36.5 ft from the end of the beams (Lines QS & QD). The strains were measured at the center of the bottom flanges of all applicable beams. The deflections were measured at the center of the top flanges of all applicable beams. In some instances the flanges of the exterior beams were too severely degraded for instrumentation to be installed.

The FEM was also used to model the bridge span behavior during truck loading conducted on the same bridge span prior to being damaged. To model the truck loadings on the undamaged bridge span, the damaged sections were removed from the bridge span model and no other changes were made to the model. The bridge span model was then subjected to four separate truck loadings that were applied on the actual bridge span.

STRAIN RESULTS

Figure 8 shows the comparison of the strain results acquired from the FEM to the experimental results of the destructive testing. A strain comparison for the results of both instrument lines, MS and QS, while Cylinder 2 was applying 62 kips to the bridge span are shown in Figure 8. It can be seen that the FEM closely simulates the strain distribution behavior of the bridge span while loaded with Cylinder 2. The FEM emulates the higher strains on the loaded beams, as well as the significant drop in strain on the damaged beams. The behavior of the beams adjacent to the damaged beams and away of from loading, in this case Beams 7 and 8, having larger strain than the damaged beams was also emulated with the FEM. The average difference in strain between the FEM and the experimental results for instrument lines MB and QB was 9.29 με.

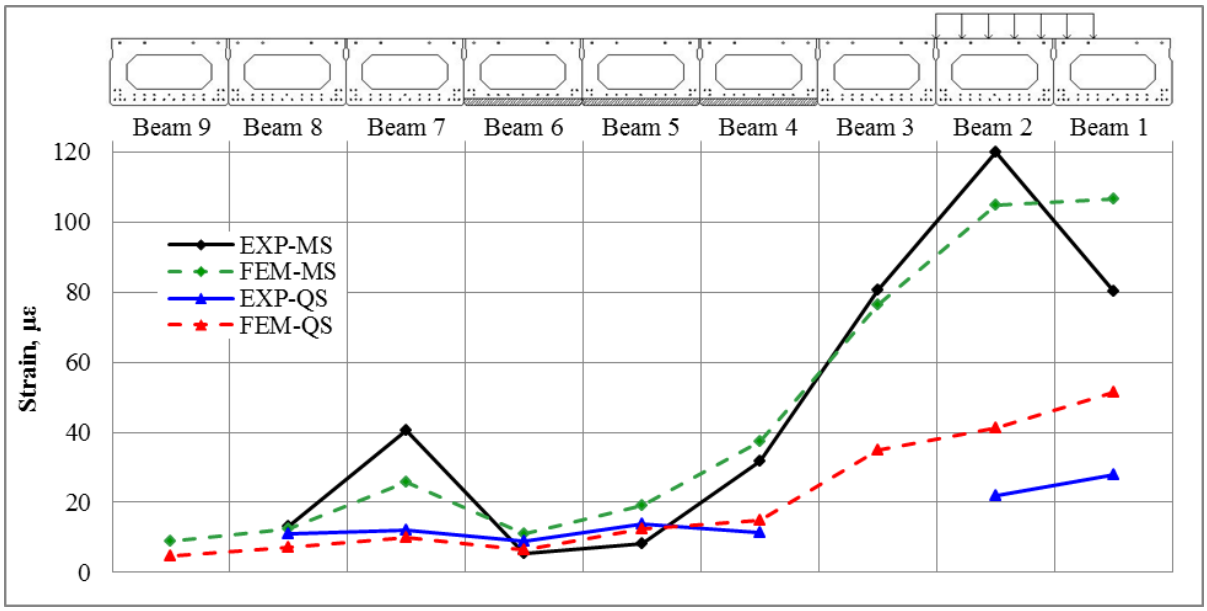

Figure 8 - FEM and experimental strain results while loaded by Cylinder 2

Displayed in Figure 9 is the strain comparison of the FEM to the experimental results for instrument lines MS and QS while Cylinder 5 was applying 73 kips to the bridge span. Figure 9 shows that the FEM was able to accurately imitate the strain distribution behavior of the damaged bridge span when load was applied to the damaged beams of the bridge span. This includes the behavior where the loaded damaged beams experienced lower relative strain values than the adjacent undamaged beams. The average difference in strain between the FEM and the experimental results for instrument lines MB and QB was 3.10 με.

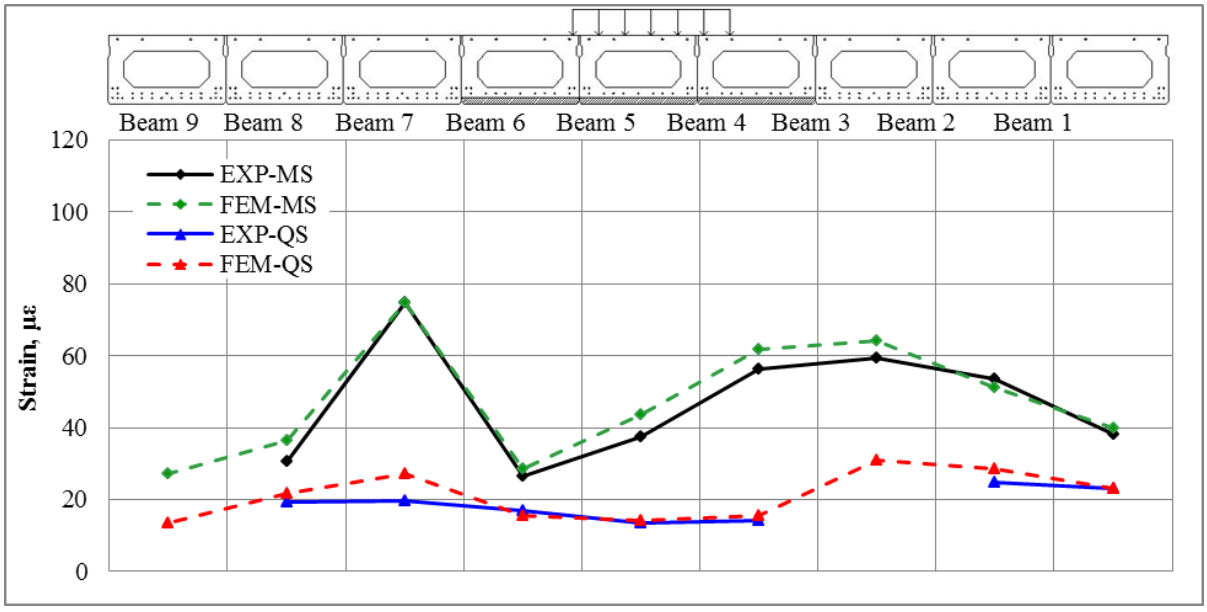

Figure 9 – FEM and experimental strain results while loaded by Cylinder 5

Presented in Figure 10 is the strain comparison of the results from the FEM and the experimental testing of the bridge span while 52 kips was applied to the bridge span by Cylinder 8. In this loading case, the FEM was able to mimic the strain behavior of the loaded beams. However, the larger relative strain of the beam adjacent to the damaged beams and opposite of the loading was not achieved. Despite the FEM being unable to model this strain distribution, the general strain distribution across the entire span provided by the FEM closely resembles the results obtained during destructive testing. The average difference in strain between the FEM and the experimental results for instrument lines MB and QB was 8.72 με.

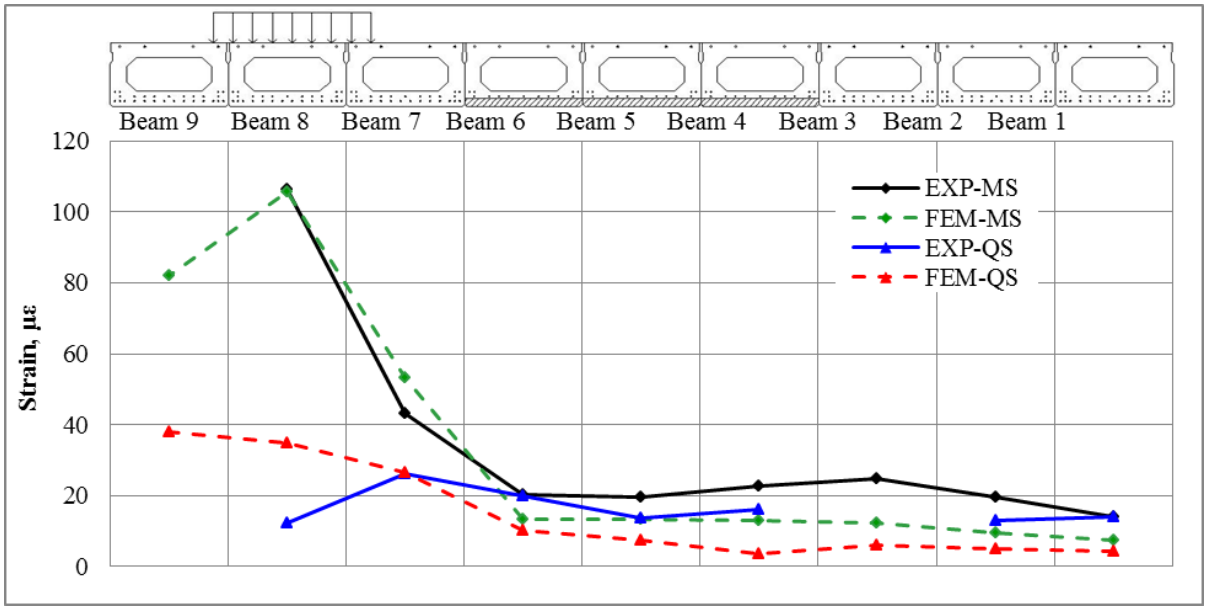

Figure 10 - FEM and experimental strain results while loaded by Cylinder 8

DEFLECTION RESULTS

Similar to the strain distribution behavior of the bridge span, the deflection profiles provided by the FEM were also compared to the corresponding deflection results from the experimental testing of the bridge span.

Figure 11 provides a comparison of the deflection results from the FEM to the results from the destructive testing of the bridge span while Cylinder 2 was applying load to the span. The deflection results yielded by the FEM were larger relative to the experimental deflection results for the beams that were in close proximity to the loading location and the opposite was true for the beams away from the loading. This behavior may be explained by the assumption made for the model that the material properties of the beams were uniform throughout the entire beam. The model does not take into account any unknown changes in the material properties of the beams. The magnitudes of the deflections are also small which makes matching the deflection results more difficult. The average difference between the deflection results of the FEM and the experimental results was 0.040 in. while the span was loaded by Cylinder 2.

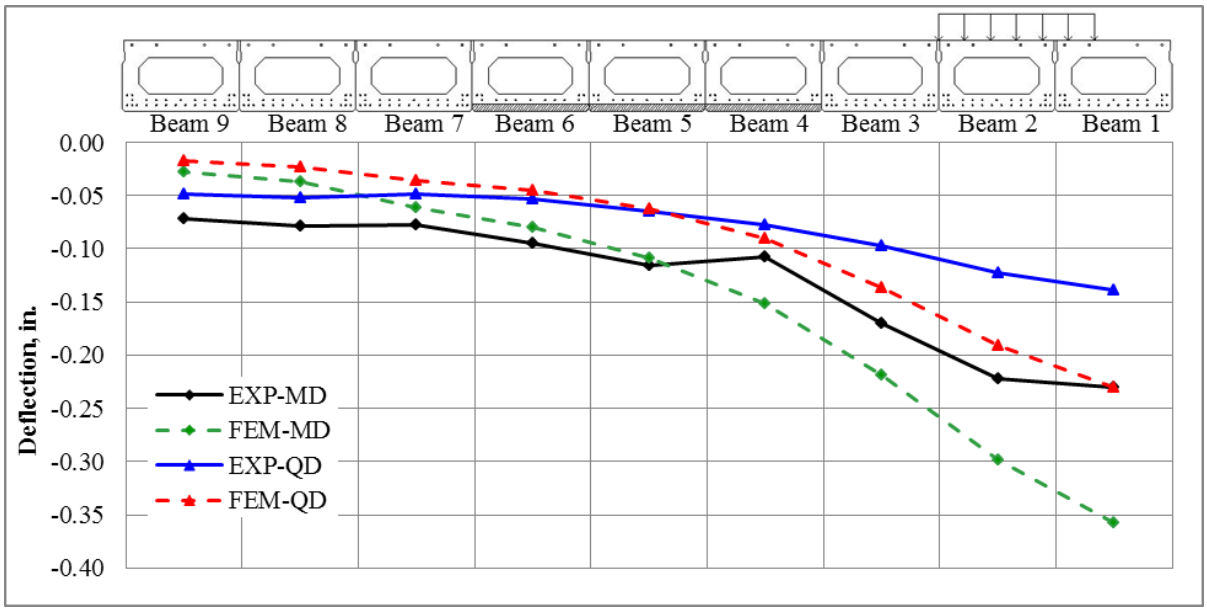

Figure 11 - FEM and experimental deflection results while loaded by Cylinder 2

Similar to when the span was loaded by Cylinder 2, Figure 12 shows that the deflection results found using the FEM were larger than the experimental results when Cylinder 5 was applying load to the bridge span. Again, this behavior may be caused by the assumptions made when developing the FEM. The results provided by the FEM offer a reasonable approximation of the general deflection profile. The average difference between the deflection results of the FEM and the experimental results while Cylinder 5 was applying load to the span was 0.042 in.

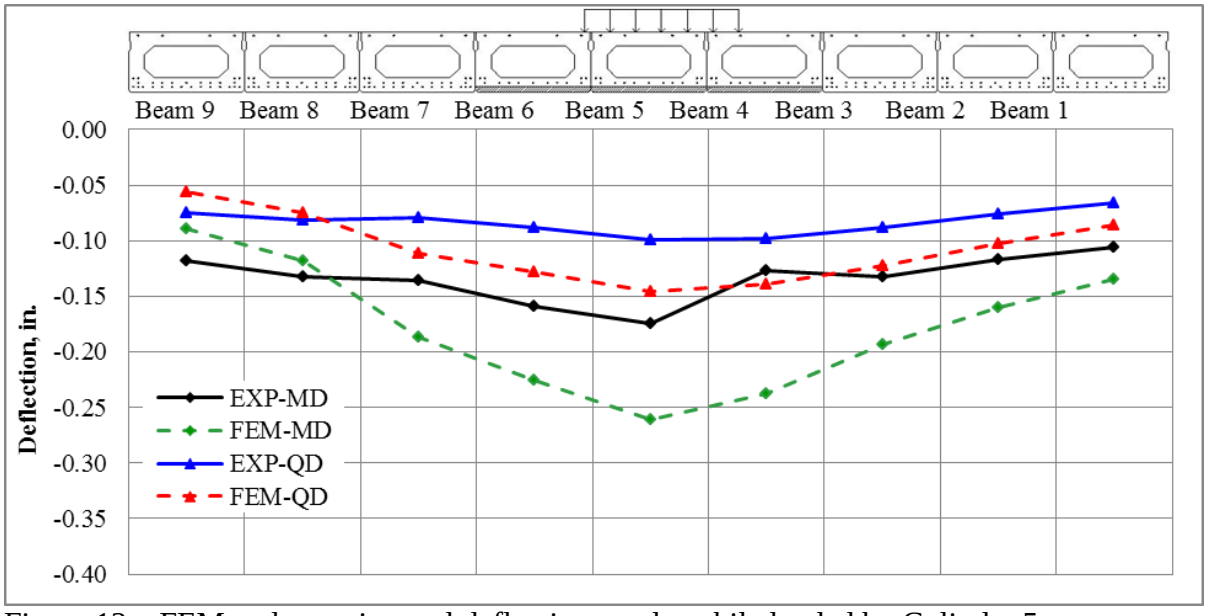

Figure 12 – FEM and experimental deflection results while loaded by Cylinder 5

Shown in Figure 13 is the comparison of the FEM deflection results to the experimental deflection results from the destructive testing of the bridge span. Similar to the previous results presented from the FEM, the FEM yielded results where the loaded beams exhibit larger magnitudes of deflection than the experiment results when the span was loaded by Cylinder 8. The deflection results from the FEM for the beams away from the load were significantly closer to the deflections from the experimental testing. The average difference between the deflection results of the FEM and the experimental results was 0.033 in. while the span was loaded by Cylinder 8.

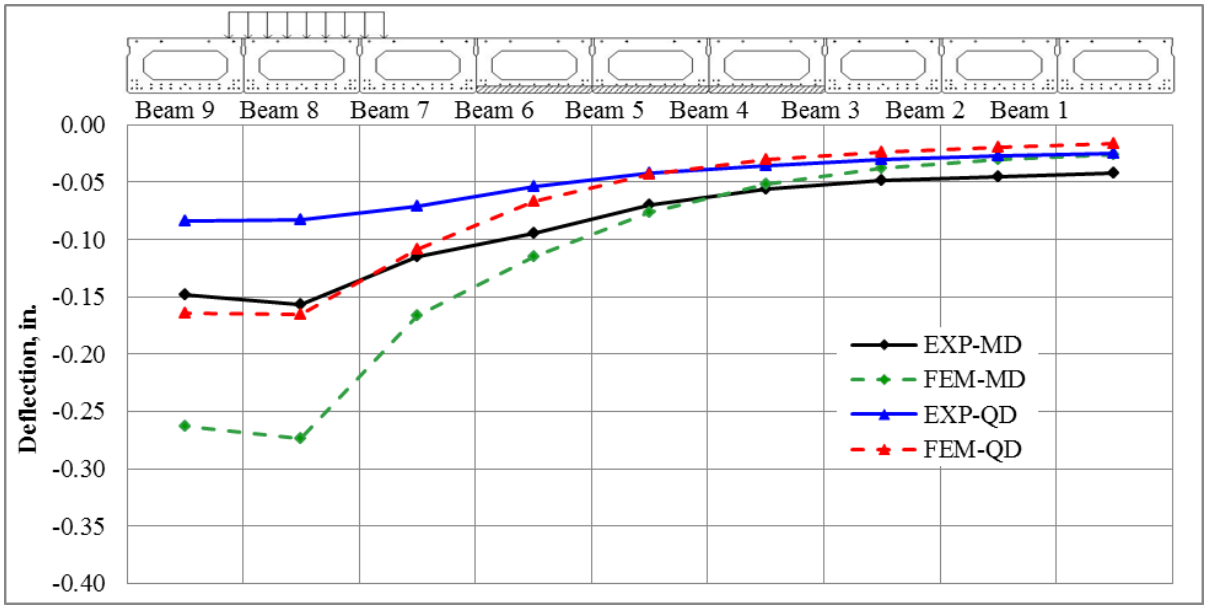

Figure 13 - FEM and experimental deflection results while loaded by Cylinder 8

TRUCK LOADING RESULTS

Presented in Figure 14 is a comparison of the strain results from the FEM and the truck testing of the undamaged bridge span. The loading locations and magnitude in truck loadings 3 and 4 were very similar and therefore the FEM and truck testing results are not provided. The undamaged bridge span model was able to emulate the general strain distribution behavior of the actual undamaged bridge span. However, the results provided by the FEM were generally smaller relative to the strain results from the truck testing. The average difference in strain between the FEM and the experimental results was 11.72 με

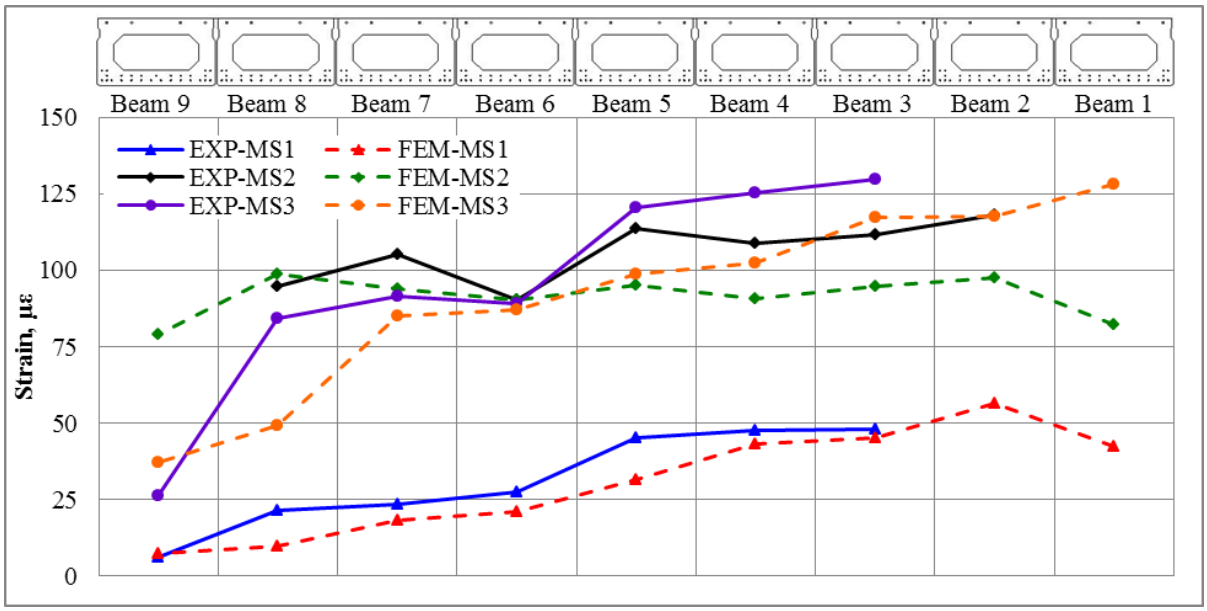

Figure 14 – FEM and experimental strain results for the truck loadings

Figure 15 displays a comparison of the deflection profiles from the FEM and the truck testing of the undamaged bridge span. This comparison demonstrates that the FEM accurately emulates the deflection behavior of the undamaged bridge span while being loaded at multiple magnitudes and at multiple locations on the span. As seen with the cylinder loadings, the beams in the FEM experience relatively higher deflections at the locations of the loads and relatively less deflection away from the location of the loading. The average difference between the deflections provided by the FEM to the experimental deflections from the three truck loadings was 0.029 in.

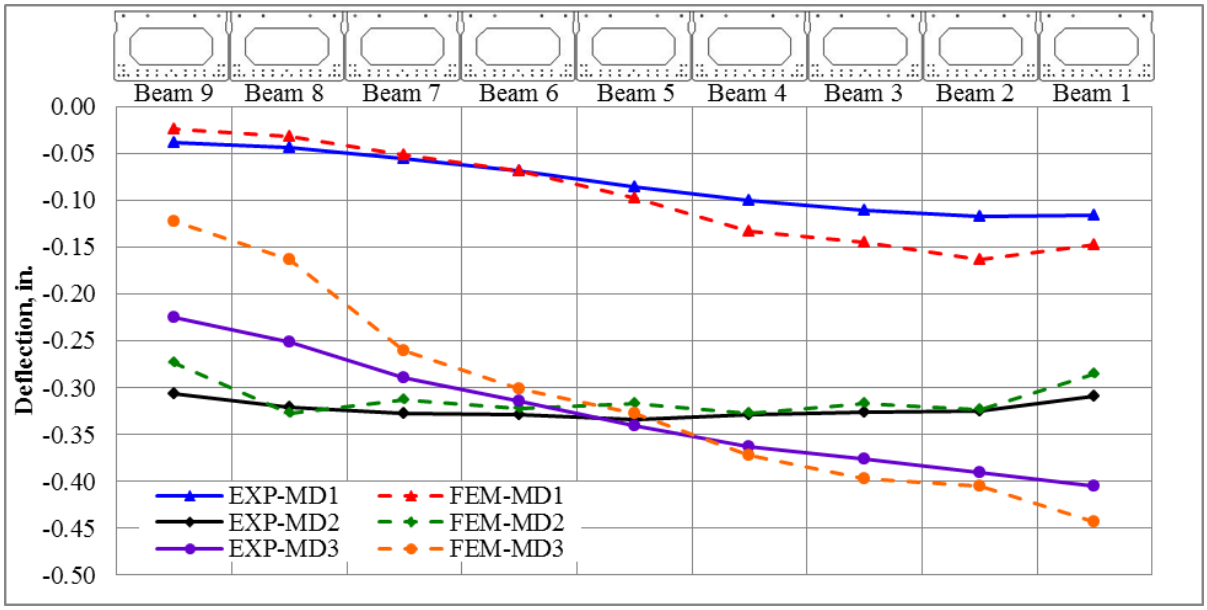

Figure 15 - FEM and experimental deflection results for the truck loadings

The strain results from the model were also used to develop distribution factors (DF) for each truck loading case. The distribution factors were calculated by taking a ratio of the largest strain of all of the individual beams to the total measured strain across the entire bridge span. Table 5 shows the largest distribution factor and which beam experienced the largest strain for each of the four truck loading cases and the three single cylinder loadings on the damaged FEM. The AASHTO LRFD distribution factors for the bridge span were also calculated for both interior and exterior beams and presented in Table 5[3]. The distribution factors calculated using the strain results from the FEM were used to calculate LRFR and LFR rating factors[3].

Table 5 – Distribution Factors for the truck loading and single cylinder load cases

	Truck Loading				Cylinder Loading		
Loading Case	1	2	3	4	2	5	8
Beam	2	8	1	1	1	7	8
Distribution Factor	0.205	0.120	0.156	0.161	0.341	0.175	0.265
AASHTO LRFD DF	0.242	0.242	0.254	0.254	-	-	-

CONCLUSIONS

It has been shown through the use of finite element modeling that the general behavior of adjacent prestressed concrete box beam bridges and individual box beams with varying degrees of deterioration can be accurately simulated. Most notably, the load distribution behavior between adjacent beams can be predicted for both damaged and undamaged bridge spans. Given sufficient load transfer mechanisms, adjacent box beam bridge systems continue to perform as a system when the bridge possesses degraded beams. However, the load distribution between adjacent beams is altered. This change in load distribution can be simulated with finite element modeling. This procedure can assist in the evaluation of other deteriorating adjacent box beam bridges.

REFERENCES

1. Huffman, J. (2012). “Destructive Testing of a Full-Scale 43 Year Old Adjacent Prestressed Concrete Box Beam Bridge: Middle and West Spans,” Masters Thesis, Ohio University, Russ College of Engineering and Technology.

2. Steinberg, E., Miller, R., Huffman, J., & Stillings, T. (2011). “Full Scale Destructive Testing of an Adjacent Prestressed Concrete Box Beam Bridge,” *PCI/NBI.* Salt Lake City.

3. Setty,C. (2012). “Truck Testing and Load Rating of a Full-Scale 43-Year-Old Prestresses Concrete Adjacent Box Beam Bridge,” Masters Thesis, Ohio University, Russ College of Engineering and Technology.

4. MacGregor, J. G., & Wright, J. K. (2005). Reinforced Concrete (4 ed.). Upper Saddle River, New Jersey: Pearson Education Inc.

5. Balakrishnan, S., Elwi, A. E., & Murray, W. D. (1988, July). “Effect of Modeling on NLFE Analysis of Concrete Structures,” *Journal of Structural Engineering*, V.114, No. 7, pp.1467-1486.

6. Barzegar, F., & Maddipudi, S. (1997). “Three-Dimensional Modeling of Concrete Structures. II: Reinforced Concrete,” *Journal of Structural Engineering*, pp.1347-1356.

7. Dassault Systemes Simulia Corporation. (2010). 12.9.2 Defining Plasticity. In *Abaqus/CAE User's Manual.* Providence, Rhode Island, USA.

8. Dassault Systemes Simulia Corporation. (2010). 20.6.1 Concrete Smeared Cracking. In *Abaqus Analysis User's Manual.* Providence, Rhode Island, USA.